



# Towards on-chip photonic-assisted radio-frequency spectral measurement and monitoring

LUIS ROMERO CORTÉS,<sup>1</sup> DANIEL ONORI,<sup>1</sup> HUGUES GUILLET DE CHATELLUS,<sup>2</sup>   
MAURIZIO BURLA,<sup>3</sup> AND JOSÉ AZAÑA<sup>1,\*</sup>

<sup>1</sup>Institut National de la Recherche Scientifique—Énergie, Matériaux et Télécommunications (INRS-EMT), H5A 1K6 Montréal, Québec, Canada

<sup>2</sup>Université Grenoble Alpes, CNRS, LIPhy, 38000 Grenoble, France

<sup>3</sup>Institute of Electromagnetic Fields (IEF), ETH Zurich, Gloriastrasse 35, Zurich 8092, Switzerland

\*Corresponding author: azana@emt.inrs.ca

Received 13 November 2019; accepted 15 March 2020 (Doc. ID 383247); published 6 May 2020

Precise detection and monitoring of the frequency spectrum of microwave signals are essential to myriad scientific and technological disciplines, including both civil and defense areas, such as telecommunications, radar, biomedical instrumentation, radio astronomy, etc. Historically, microwave engineering has provided solutions for these tasks. However, current radio-frequency (RF) technologies suffer from inherent shortcomings that limit their capability to provide agile (e.g., real-time) measurements over a large operation bandwidth in energy-efficient and compact (e.g., integrated) formats. Overcoming these limitations is key to fulfilling pressing performance requirements in the above-mentioned application fields, as well as for compatibility with platforms that require chip-scale integration and/or low weight and dimensions, such as satellites and drones. Integrated microwave photonics is an emerging field that leverages the advantages of optical technologies for realization of microwave operations with high bandwidth, low power consumption, and increased agility and flexibility in on-chip platforms, offering an alternative path for integration of advanced RF processing and analysis methods in mature semiconductor technologies. This mini review surveys some of the latest advances in microwave spectral measurement and monitoring techniques realized through photonic approaches, with a special focus on methods suitable for on-chip integration. © 2020 Optical Society of America under the terms of the OSA Open Access Publishing Agreement

Access Publishing Agreement

<https://doi.org/10.1364/OPTICA.383247>

## 1. INTRODUCTION

Microwave signals—typically defined as frequencies in the 300 MHz to 300 GHz range—have been extensively exploited over almost a century for myriad fields of fundamental science and applied technologies [1]. In its origins, the capability to generate and measure radio-frequency (RF) signals opened the path to long-range communication systems, before the advent of optical fiber transmission [2]. Nowadays, these technologies are used widely in both civil and defense disciplines, such as in telecommunications, radar, navigation, astronomy research, spectroscopy and sensing, biomedical fields, etc. [3,4].

In particular, accurate and reliable detection and measurement of microwave signals are key for technologies tackling these application areas, as the quality of the measurement ultimately limits the performance of the system in virtually every scenario [5]. This is especially important in situations where detailed information of the signal under test (SUT) is required. Operations that require characterization of the frequency content of the SUT are fundamental for a wide range of applications. Such measurements provide key information, typically unavailable or difficult to obtain through other means, including, for instance, the location of the

SUT in the overall RF spectrum, information on the occupied spectral resources, identification of interferences or other undesired signals, etc. Specific applications may require monitoring of the complete SUT frequency spectrum, or information about some of its properties, such as its central frequency or bandwidth.

The arrival of new-generation mobile communications, radars, and other microwave-based systems demands high-performance RF measurements, posing critical challenges to current microwave systems [3–10]. These applications require RF spectral measurements that extend over a very broad frequency range, e.g., well above a few GHz, and with a superior performance, e.g., in terms of frequency resolution, sensitivity, etc. In many practical cases, the desired frequency-domain information should be obtained in a rapid and agile fashion, even in a real-time manner [3–12]. Finally, emerging applications also require that the measurement techniques can be implemented in platforms with a very low size, weight, power consumption and cost, often labeled as the SWaP-C factor. This latest requirement is particularly critical for applications that involve the use of satellites, unmanned aerial vehicles (drones), etc. [13]. However, microwave technologies have shown limited potential to achieve the desired high performance, including agile and high-quality measurement capabilities

over broad bandwidths, with a reduced footprint. State-of-the-art RF technologies are inherently constrained by the relatively low instantaneous frequency bandwidth of the electronics [5]. A key limitation in this regard concerns the speed of available analog-to-digital converters (ADCs), for which direct digitization of microwave signals in the high microwave range, e.g., above 20 GHz, becomes challenging [14]. Additionally, the RF receivers presently used for measurement tasks tend to be bulky, power-hungry systems with limited hardware capabilities. This is due mainly to the poor compatibility of current RF components with large-scale integration, resulting in systems with high SWaP-C factors [15–18].

The field of microwave photonics (MWP) represents a promising alternative towards future RF technologies [19–21]. This prominent field leverages the unique advantages of photonics to overcome crucial limitations of present microwave systems. Figure 1 shows a basic illustration of a general MWP system. In particular, MWP has been shown to provide unprecedented performance capabilities for modern microwave measurement techniques, including, among others, large instantaneous frequency bandwidths and/or broadband reconfigurability (well above the GHz range), ultralow noise operation, and chip-scale integration with high energy and cost efficiency, enabling significant SWaP-C reductions [15–18]. Another important inherent advantage of MWP technologies is their increased immunity to electromagnetic interference. This set of features would be challenging or simply unattainable for current microwave technologies.

Pioneering work demonstrated the potential of MWP solutions to provide important performance improvements over conventional RF technologies [19,20]; however, this often came at the expense of lower reliability and the need for km-long optical fibers and/or bulky and costly optical components, thus practically worsening SWaP-C and robustness. In the attempt to address this issue, over the last decade, we have witnessed a clear transition in the general field of MWP towards integrated photonic implementations [15–18], promising to improve performance and SWaP-C. Important progress has also been reported towards the realization of programmable MWP processors in integrated formats [22]. The reader can find detailed information on the state of the art in the field in the following recent comprehensive review papers: [15–18,23]. Indeed, numerous MWP solutions have been demonstrated in a variety of integrated photonics platforms, including indium phosphide (InP) [24], silicon nitride [25], and perhaps

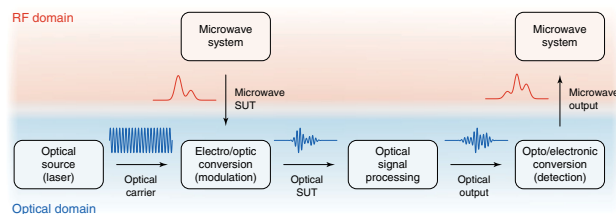


**Fig. 1.** General description of a MWP system. A microwave system generates a SUT to be processed. An optical carrier is modulated with the microwave SUT and manipulated by an optical signal processing system, implementing the desired operation. The resulting optical signal is then converted back to the microwave domain via a detection process. In the particular case of radio-frequency spectral measurement and monitoring, the combined effect of the optical signal processing system and opto-electronic conversion is designed to implement the desired analysis functionality on the microwave SUT.

most interestingly, silicon photonics (SiP). This latest technology is especially attractive for its compatibility with mature micro-electronic complementary metal-oxide-semiconductor (CMOS) foundries, enabling realization of photonic devices with excellent processing control and low fabrication cost [15–18,26]. Research in this direction has flourished in recent years, opening a promising alternative to integration of advanced RF measurement equipment on a chip, a critical feat across the above-mentioned application fields.

This mini review surveys some of the latest advances in RF spectral measurement and monitoring technologies enabled by MWP, with special emphasis on solutions realized in integrated formats. The paper is structured as follows: Section 2 reviews the latest advances in photonic implementation of broadband/multiband scanning RF receivers, with particular attention to the efforts made towards chip-scale integration. These receivers can capture the frequency content of a microwave SUT by scanning its spectrum. This is an effective and widespread approach for wideband spectral measurement; however, the need for a frequency scan may affect the capability to achieve real-time operation. In order to circumvent this limitation, optical signal processing approaches based on frequency-to-time mapping have been proposed, as reviewed in Section 3. These approaches can achieve ultrafast characterization of the full spectral content of RF signals, but they typically rely on bulky photonic devices (e.g., optical fibers) that limit their feasibility for chip-scale integration. However, many practical applications do not require a complete characterization of the full frequency spectrum of the SUT. A relevant case is that of instantaneous RF measurement (IFM) systems, which aim to obtain information on the central frequency of the incoming signal only. Towards this aim, integrated MWP solutions have proven successful in achieving high performance with compact footprints. Section 4 reviews the latest developments in photonics-based on-chip IFM systems.

## 2. COMPACT BROADLY TUNABLE PHOTONICS-BASED RF RECEIVERS

Broadband and multiband RF receivers capable of performing spectral analysis of incoming RF signals in an agile and user-defined fashion are critical enabling components in many important applications, such as for multi-standard communications, cognitive radio, or electronic defense [7]. An effective and agile solution is to scan the whole SUT spectrum through fast tunable down-conversion [3,7]. This requires a single broadly tunable heterodyne receiver consisting of (i) a wideband mixing stage, (ii) a broadly tunable RF local oscillator (LO), and (iii) a broadly tunable image-reject bandpass filter (IRF). The receiver would down-convert the portion of the spectrum adjacent to the LO (within the filter bandwidth) to intermediate frequency (IF), where an ADC with relaxed performance requirements would acquire the low-frequency down-converted SUT.

Nowadays, there is an urgent need to identify and develop alternative concepts and technological solutions for chip-scale integration of such receivers, in order to reduce their SWaP-C, while increasing their hardware capabilities. Unfortunately, current RF crystal oscillators—or phase-locked loops—and bandpass cavity filters with broadband tuning capability are not feasible for on-chip integration, preventing the realization of a compact scanning receiver. Moreover, the operation bandwidth of such

a receiver would be severely limited by the bandwidth of the RF mixer [3,7]. To overcome these limitations, current solutions exploit channelization receivers that decompose the broadband SUT into multiple channels by means of an RF filter bank. The problem in turn is that the volume of the filter bank increases dramatically with the number of channels (i.e., with the measurement frequency bandwidth) [3,4,7]. Alternative designs have been proposed using entirely different physical principles, and this has enabled, e.g., the demonstration of on-chip spectroscopes operating over a large frequency range (up to  $\sim 300$  GHz) using purely electronic circuits [27]. However, these designs require a significant post-processing of the measured data, affecting their capability to achieve the measurement agility and speed that is needed in many practical cases.

Recently, MWP coherent architectures have been exploited to achieve extremely wideband RF mixing while avoiding the use of RF filter banks in the receiver design [19,21]. In addition, the photonics implementation provides a solid path for chip-scale integration of the resulting schemes, beyond the potential of conventional RF components [17]. Recent progress in this direction is reviewed in the following.

In an MWP coherent framework [21,28,29], the broadband RF SUT is first up-converted to optical frequencies by modulating a continuous-wave (CW) optical carrier (OC) in an electro-optic (EO) amplitude modulator (AM), as illustrated in Fig. 1. Then, a portion of the detected spectrum is selected via optical processing, e.g., through an optical IRF with bandwidth of a few GHz, or optical “in-phase” and “quadrature” (I/Q) demodulation. Finally, the selected portion of the spectrum is coupled with an optical LO tone set at a suitable frequency, and converted back to baseband through mixing in a photodiode. A key parameter to manage in this approach is the phase noise between the OCs used in the schemes. In order to preserve the RF input signal integrity, the OC and the

tunable optical LO must be phase locked; otherwise the phase noise between them dramatically corrupts the down-converted signal [30]. Techniques for reduction of optical noise contributions in the system exist, but they face limitations in their compatibility with an effective chip-scale integration, as described in what follows.

### A. Simple Self-Heterodyne Architectures

The simplest solutions for achieving low-phase-noise photonics-assisted RF receivers stem from the use of optical self-heterodyning [see Fig. 2(a)]. This technique exploits a single OC laser, and the optical LO is derived from the OC through amplitude modulation (inset II), e.g., by means of an EO modulator (AM<sub>2</sub>) driven by a tunable RF tone [21,28,29].

Although straightforward, methods based on self-heterodyning present a strong drawback: they require a synthesizer (or multiple crystal oscillators) at the input of the EO modulator (AM<sub>2</sub>) to generate the tunable optical LO. This prevents a reduced form factor, making them unsuitable for chip-scale integration.

### B. Optical-Frequency-Comb-Based Receivers

In order to avoid the use of the RF synthesizer, alternative solutions use an optical frequency comb as the LO for the down-conversion operation [29,31–35] [see Fig. 2(b)]. Recall that an optical frequency comb (OFC) is a spectrum consisting of discrete frequency components periodically separated by a frequency spacing known as the free spectral range (FSR). For example, in a self-heterodyne scheme, Fig. 2(a), the comb generator replaces the EO amplitude modulator. As a comb generator, a cavity-less structure is generally preferred, due to its higher compactness and increased robustness to environmental instabilities [31]. These are composed of a cascade of EO amplitude and phase modulators driven by a single, low-frequency

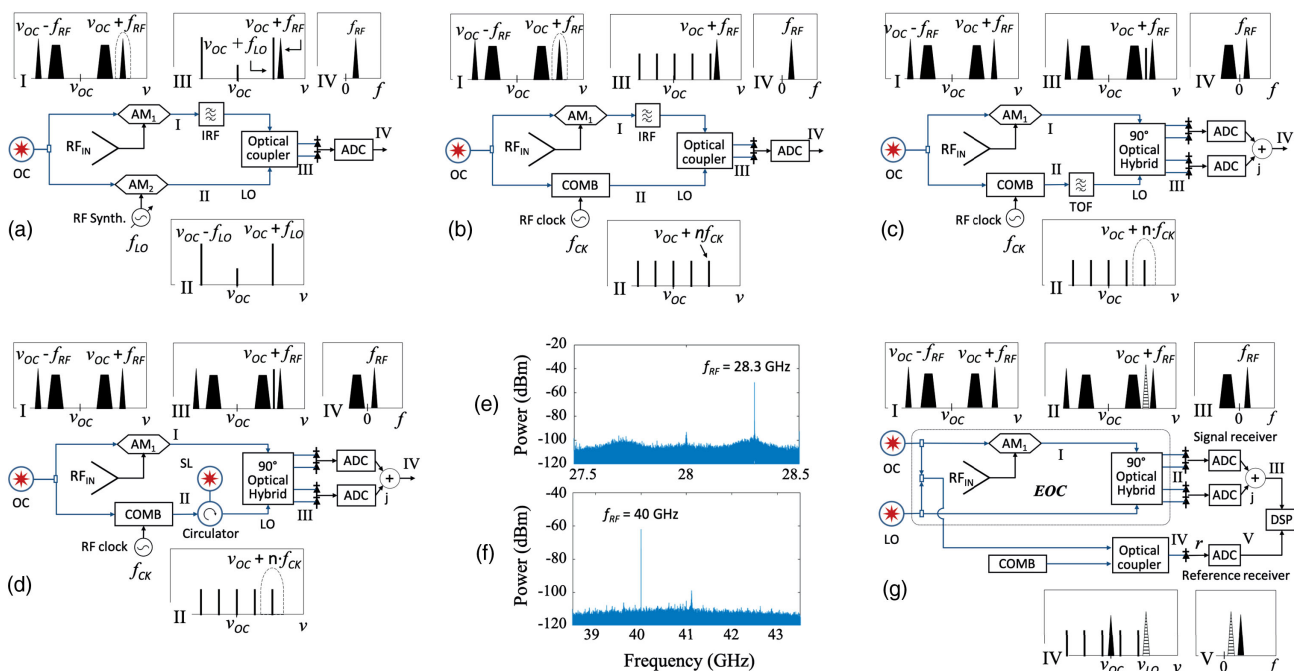


**Fig. 2.** (a)–(d), (g) MWP coherent architectures. Insets depict optical or RF signals at different points. (e), (f) Power spectrum of the noise-free reconstructed SUT, produced by the injection-locking-based receiver of scheme (d) [31], and the FF receiver with SiP modulator of scheme (g) [32], respectively, when 28.3 and 40 GHz tones are used as input. OC, optical carrier; LO, local oscillator; AM, amplitude modulator; IRF, image-reject filter; TOF, tunable optical filter; EOC, electro-optic converter.

RF oscillator at a fixed frequency,  $f_{CK}$ . When the generator is fed by the OC at a frequency  $\nu_{OC}$ , a coherent OFC with central frequency  $\nu_{OC}$  and FSR  $f_{CK}$  is generated (inset II). The  $n$ -th comb line, which is the closest in frequency to the filtered output of  $AM_1$ , acts as the optical LO at frequency  $\nu_{LO} = \nu_{OC} + n f_{CK}$  for the down-conversion at IF (insets III and IV). However, because the scheme stems from generating the OFC from the OC, only half of the resulting comb lines are *de facto* usable for the down-conversion, so, this inefficiency leads to difficulty in achieving a wide operating bandwidth [35].

### C. RF Filtering Based on Optical I/Q Demodulation

The second main issue concerning coherent MWP receiver approaches arises when the microwave application requires high filtering performance [3,7], with specifications that may be difficult to attain using the optical IRF approach at the core of (self-)heterodyne detection schemes [Figs. 2(a) and 2(b)]. In fact, albeit optical narrow bandpass filters can be achieved in very compact formats if implemented using integrated technology, at present, they show limited out-of-band rejection ( $\sim 30$  dB), high insertion loss ( $> 10$  dB), low rate of roll-off ( $\sim 20$  dB/GHz), and poor thermal stability [29].

Alternatively, optical I/Q demodulation can be used for narrow bandpass filtering and image rejection in lieu of the IRF [Fig. 2(c)] [31–35]. If the I/Q imbalance is properly compensated for, image and out-of-band rejection over 40 dB can be achieved [36]. However, these schemes require a tunable optical filter (TOF) to extract a single comb line for the baseband down-conversion and suppress the other lines ( $> 40$  dB for most practical applications) in order to avoid channel crosstalk as well as phase-to-amplitude conversion at the output of the receiver [31–35]. The TOF requires a lower performance, in terms of flatness and roll-off ratio, than the IRF, but a reduced out-of-band rejection ( $\sim 30$  dB) could lead to an equivalent (and insufficient) level of channel crosstalk. Moreover, through this approach, the receiver is able to scan the input spectrum only at discrete steps, affecting the flexibility offered by the scheme [35].

### D. Optical Injection Locking for Filtering of Comb Lines

A filtering approach based on optical injection locking can improve the crosstalk performance of the previous technique [see Fig. 2(d)] [31,34]. By injecting the whole OFC generated by the OC into the cavity of a slave laser, i.e., the LO laser, the latter is forced to match the OC's frequency and phase, also inheriting its phase noise characteristics. This way, the LO laser is phase locked with the OC during the OC-LO detuning. As an example, Fig. 2(e) shows the power spectrum of the OC-LO noise-free signal acquired by the receiver in Ref. [31], using a 28.3 GHz tone as the input. In this approach, the comb line within the locking range of the LO laser is amplified while the other lines are greatly suppressed. In Refs. [31,34], a series of two injection locking stages is exploited to achieve a channel crosstalk below 40 dB. Some drawbacks are introduced, however, as a consequence of the injection-locking process; this technique requires precise alignment of the involved lasers, and is ultimately affected by their linewidths, the injection power, and environmental instabilities, posing a serious tradeoff between performance and robustness [31,35]. Moreover, current optical circulators, which are essential for injection locking, are not

suitable for monolithic integration, limiting the foreseen on-chip realization and related footprint reduction [37].

### E. Receivers Based on Digital Feed-Forward Laser Noise Cancelling

In Ref. [35], a novel design of a MWP receiver with digital feed-forward laser noise cancellation was proposed to overcome the main drawbacks of the previously described schemes. This novel design uses two independent free-running lasers as OC and LO [see Fig. 2(g)]. The method stems from recording at IF the OC-LO beating noise that affects the baseband output of the signal receiver by means of a second receiver, i.e., the reference receiver. The reference signal (signal  $r$  in inset V) contains information about the frequency detuning position between the OC and LO lasers, as well as about their differential beat noise (in both amplitude and phase). This information is then exploited to reconstruct a noise-free representation of the incoming RF signal through a simple digital signal processing (DSP) algorithm [35]. In more detail, at the EO converter (EOC), both the OC and LO are split to be coupled together in a 3 dB optical coupler. The coupled signals are sent to the reference receiver by an optical fiber, where they are heterodyned with an OFC using another optical coupler (inset IV) and photodiodes. The electrical output of the photodiodes (signal  $r$  in inset V) is digitized and used by the digital feed-forward algorithm.

In the proposed solution, the performance and integration capability improvement rely on the following key features. First, the OFC acts only on the reference receiver; as a result, no optical filtering of the comb lines is required, leading to the following benefits: 1.i. the channel crosstalk is cancelled out because the signal receiver is completely isolated from the OFC; 1.ii. the thermal stability and the photonic-integration capability are improved due to the absence of optical filters or injection-locking mechanisms; 1.iii. this design inherently enables a continuous tunability because no filtering or locking-range bandwidth are involved. Second, the OFC generator is outside the signal receiver; as a result: 2.i. the chip-scale integration of the EOC is greatly simplified; 2.ii. since all interferometric structures susceptible to vibrations are contained within the EOC, this would provide high mechanical stability when they are realized through photonic integrated technology. Third, the OFC is independent of the OC and LO lasers; this way: 3.i. the scheme is able to fully exploit the frequency lines provided by the OFC, and the receiver can potentially reach a much wider RF input range; 3.ii. the OFC generator can be implemented through different techniques, e.g., EO modulation or mode locking.

In recent work, the feed-forward noise-cancelling architecture has enabled the realization and experimental demonstration of the first on-chip broadly tunable RF scanning receiver, using SiP technology [38]. The device was fabricated using a multi-project-wafer service, and it achieved ultralow-noise operation in the frequency range of 0–35 GHz, with an unprecedented image rejection  $> 80$  dB. A key element in the demonstrated scheme is a traveling-wave, push-pull, SiP Mach-Zehnder modulator, which shows a noise-reduced operation in the mentioned frequency range and above, combined with a linearity performance comparable to those obtained using standard lithium niobate technology [32]. As an example, Fig. 2(f) shows the power spectrum of the OC-LO-noise-free reconstructed signal when an RF tone at frequency  $f_{RF} = 40$  GHz is used as input [32].

### 3. FREQUENCY-TO-TIME MAPPING FOR REAL-TIME SPECTRAL ANALYSIS OF MICROWAVE SIGNALS

Widespread microwave applications such as advanced telecommunications, radar, astronomy observations, and biomedical imaging and sensing require the capability of dynamic monitoring of the RF spectrum, involving measurement solutions that can enable spectral analysis in real time [3,4,6–12]. Scanning receivers, such as those reviewed in Section 2, are inadequate for high-speed spectral analysis of broadband RF signals with fast frequency variations, due to their relatively slow refresh rate and the related poor probability of interception. Real-time spectral analysis entails the capture of the entire frequency content of the SUT in a single, fast measurement. Optical signal processing has provided promising solutions for realization of this task. An inherent advantage of photonic solutions is that they provide easy access to measurement capabilities over ultra-broad instantaneous frequency bandwidths, even exceeding the THz range [39–42]. However, spectral measurements over such large bandwidth in a real-time fashion requires the use of advanced strategies.

Towards this aim, an important set of demonstrated MWP techniques relies on the modulation of an OC by the RF SUT followed by a frequency-to-time mapping (FTM) process (optical signal processing box in Fig. 1), allowing one to capture the SUT spectrum information directly in the time domain. In the following, we provide a review of conventional and recent developments of real-time RF Fourier analysis based on FTM.

#### A. Conventional Methods for FTM-Based Spectral Analysis

Several methods for FTM of RF signals on an OC have been proposed, most of which rely on the application of dispersive Fourier transform and the time lens concept.

##### 1. Dispersive Fourier Transform

The fundamentals of the dispersive Fourier transform—or dispersive FTM (D-FTM)—are derived from the so-called space–time duality [43–46]. This establishes a formal similarity between the linear operators that describe Fresnel diffraction and second-order group velocity dispersion (GVD). In free-space optics, it is possible to obtain the Fourier transform of the transverse wavefront profile of a wave in the far-field propagation regime [47]. The space–time duality allows for a similar process to occur in the time domain: an optical pulse propagating through a medium exhibiting a certain amount of GVD is re-shaped into a temporal waveform that resembles its own frequency spectrum [48,49]. Optical GVD (particularly, second-order GVD) occurs in a transparent medium in which the different frequency components of the input signal propagate through the medium at different speeds, following a linear group delay versus frequency distribution [47,50,51]. Figure 3(a) illustrates this duality.

Intuitively, the FTM process arises from the fact that each spectral component of the SUT arrives at the output of the dispersive medium at a different time, thus mapping the SUT's frequency content to the time domain [see Fig. 3(a)]. For a brief mathematical analysis, we consider the case of an optical pulse with complex envelope  $E_i(t)$  that propagates through a transparent, second-order GVD medium in the linear regime. In this case, the output

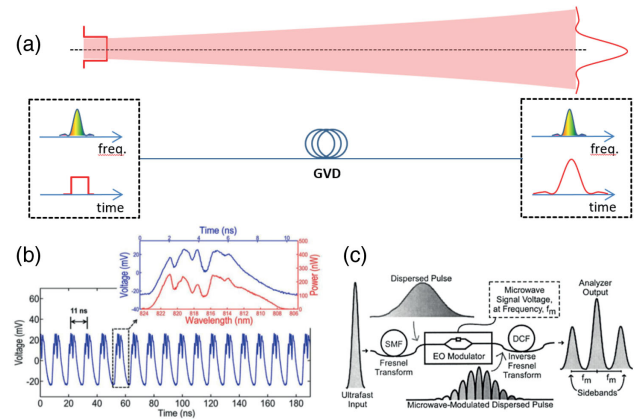


**Fig. 3.** Space–time duality and D-FTM. (a) Equivalence between the diffraction in the far field of an input spatial wavefront and the propagation of an input temporal waveform through GVD, leading to D-FTM. (b) Example of D-FTM: the temporal waveform of a pulse recorded by an oscilloscope precisely maps the pulse spectrum measured by a conventional optical spectrum analyzer. Reproduced under the terms of the CC-BY Creative Commons Attribution 4.0 International License [52]. Copyright 2012, Macmillan Publishers Limited (now Springer Nature). (c) Principle of Fourier analysis of RF signals by combining the modulation of a chirped light pulse, with dispersive propagation. Reprinted with permission from [53] © The Optical Society.

waveform exhibits a temporal envelope given by the following equation [51]:

$$E_o(t) = e^{i \frac{t^2}{2\beta_2 z}} \int_{-\infty}^{\infty} E_i(\tau) e^{i \frac{\tau^2}{2\beta_2 z}} e^{-i \frac{t\tau}{2\beta_2 z}} d\tau, \quad (1)$$

where  $t$  is the time variable,  $\beta_2$  is the second-order dispersion coefficient (the second-order derivative of the wave-vector with respect to radial frequency), and  $z$  is the propagation length of the wave in the medium. Note that the effects of attenuation, latency, and higher-order dispersion are neglected for simplicity.

Provided that the so-called temporal Fraunhofer—or temporal far-field—condition is satisfied,  $|\beta_2|z \gg \Delta t^2/2\pi$  (where  $\Delta t$  is the total duration of the input waveform), the  $\tau^2$  term in the integral of Eq. (1) can be neglected, and  $E_o(t)$  becomes proportional to a scaled version of the Fourier transform of  $E_i(t)$ , with an additional time-dependent quadratic phase factor. The intensity of the waveform at the output of the dispersive medium maps then the power spectrum of the input waveform along the time domain [48,49]. The FTM law (i.e., the scaling factor between the time axis of the output waveform, and the frequency axis of the input spectrum) writes  $t \leftarrow -4\pi\beta_2 z\nu$ , where  $\nu$  is the frequency variable. A less restrictive condition, called the antenna designer's formula, can also be used as an approximation of the far-field regime condition:  $|\beta_2|z > \Delta t^2/\pi$  [54].

Owing to its simplicity—only a transparent optical medium with suitable GVD is required—this D-FTM realization has been extensively used in various domains of science and engineering, including real-time spectroscopy [55], high-speed microwave spectrum sensing [56], ultrafast metrology and imaging [52,57,58], and many others [59]. Particularly relevant for the purposes of this review, the principles of D-FTM have been applied to real-time Fourier transform of RF signals. First, the RF SUT modulates a light wave with a flat spectral phase (e.g., a CW laser). Then, the modulated optical signal is sent through a dispersive line (optical

signal processing block in Fig. 1). The output instantaneous power follows the power spectrum of the RF SUT mapped along the time domain [see Fig. 3(a)]. Various kinds of dispersive media have been used for implementation of D-FTM [57], the simplest one being a single-mode fiber (SMF) section [60]. This medium exhibits a relatively modest GVD ( $\sim 17$  ps/nm/km at 1550 nm [61]), such that the D-FTM typically requires a long fiber section to provide the prescribed amount of dispersion, resulting in detrimental losses, higher-order dispersion, and polarization mode dispersion. Alternatively, dispersion-compensating fibers can offer higher GVD values (e.g., 120 ps/nm/km at 1550 nm [53]). Linearly chirped fiber Bragg gratings (LC-FBGs) are an attractive alternative, as they can provide large amounts of GVD in a compact format [62]. As such, LC-FBGs have thus been extensively used for MWP applications [49,63]. Other solutions based on spatial dispersion have been also demonstrated, including diffraction gratings [50] and chromo-modal dispersion in multimode optical waveguides [64].

It should be noted, however, that the far-field condition requirement of the D-FTM imposes inherently stringent constraints. Achieving the required amount of GVD can be quite demanding, potentially requiring long propagation distances and the associated high losses, which may need to be compensated for through simultaneous re-amplification of the propagating light wave [65]. More importantly, the far-field condition imposes severe tradeoffs on the performance specifications of the technique, most prominently, on the maximum duration of the input optical waveform, or equivalently, the minimum achievable frequency resolution (i.e., the minimum frequency difference identifiable between time-mapped frequency components), and the related time-bandwidth product (TBP, the ratio of the SUT's full bandwidth to its frequency resolution, serving as a metric for the "number of resolvable frequency bins" in the performed spectral measurement). For example, let us consider using a 1 km long section of SMF-28 as the GVD medium at 1550 nm; the duration of the input light pulse—modulated by the RF SUT—should not exceed 7 ps, corresponding to a frequency resolution larger than 150 GHz. This would be clearly impractical for most microwave applications; in fact, spectral analysis of signals with a frequency resolution below the tens-of-GHz range would require extremely large, possibly unreachable, amounts of GVD. On the other hand, the key advantage of optical GVD media is that they can provide extremely large processing bandwidths, in the THz range and above. D-FTM of nanosecond-long RF signals has been directly implemented in the microwave domain, i.e., using microwave dispersive lines based on microstrip chirped electromagnetic bandgaps [66], but this cannot be easily scaled for operation over frequency bandwidths exceeding just a few GHz. Finally, D-FTM techniques are intrinsically limited in terms of latency time, which is ultimately set by the propagation time of the waveform through the dispersive medium, about 5 ms per km of single-mode optical fiber.

## 2. Time Lens Approach

To circumvent these limitations, D-FTM can be applied in a different configuration, namely, by modulating the RF SUT onto a linearly chirped optical waveform, prior to dispersive propagation [67,68]. The system can be designed so that the introduced GVD perfectly compensates for the phase of the original chirped optical pulse by canceling the  $\tau^2$  term in Eq. (1) [53]. This configuration, known as near-field FTM [69], has been demonstrated to achieve

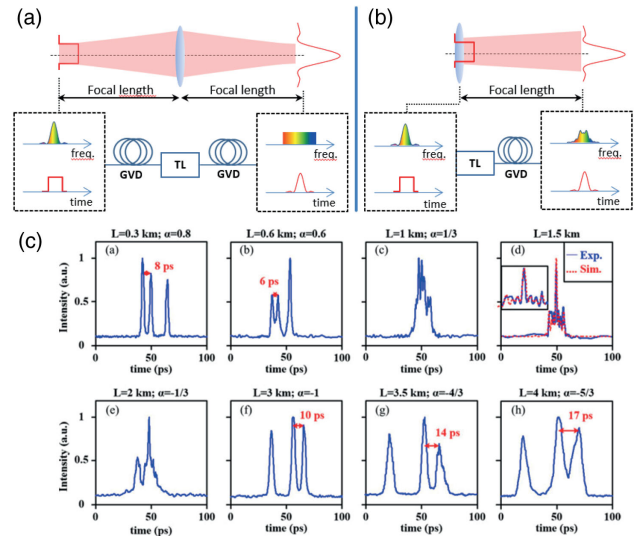


**Fig. 4.** (a) Fourier analysis by means of the  $2f$  setup in the space (top) and time (bottom) domains. GVD and TL are respectively equivalent to free-space propagation and a thin lens. (b) Simplified setup for Fourier analysis, where the first dispersion step is omitted [71]. (c) Example of spectral analysis of a digital RF input signal modulated on an optical carrier based on the combination of an electro-optic TL and a dispersive fiber. The blue traces represent the intensity of the waveform along the fiber. At the proper propagation distance ( $L = 1.5$  km), the intensity maps the spectrum of the RF SUT. Reprinted with permission from [72] © The Optical Society.

FTM of significantly longer RF signals (as long as a few ns, corresponding to sub-GHz frequency resolutions), while relaxing the GVD requirements.

The multiplication of an optical waveform by a linear chirp term can be interpreted as the temporal analog of a thin lens in free-space optics [70]. The implementation of this so-called time lens (TL) has led to new design architectures for real-time spectral analysis, such as the temporal  $2f$  setup (GVD–TL–GVD) shown in Fig. 4(a) [73]. This scheme has the advantage of forming the exact Fourier transform (in both amplitude and phase) in the temporal focal plane of the TL [47]. The time-domain processing setup consists of a TL between two suitable GVD propagation lengths [74] [see Fig. 4(a)]. When only the power spectrum of the RF SUT is needed, the input GVD line can be omitted [69,71,72,75], as illustrated in Fig. 4(b).

In general, as compared to the basic D-FTM scheme, Fourier processing techniques based on the TL approach offer an improved frequency resolution, e.g., into the sub-GHz range, but at the cost of a more complex implementation, as they typically require additional optical active components, high-power laser sources, and precise temporal timing control. Different realizations of the TL have been demonstrated: by driving an EO phase modulator with a quadratic voltage signal [76], by exciting four-wave mixing (FWM) with a linearly-chirped pump pulse [77], or by cross-phase modulation with a parabolic-shaped pump pulse [78]. Nonlinear TLs have been demonstrated to significantly outperform their EO counterparts [73], in terms of frequency chirp value (slope of the linear frequency variation along the time axis) and temporal aperture (duration over which the lens imposes the desired frequency chirp) [46]. A higher-frequency chirp translates into a smaller amount of dispersion in the Fourier transformer design, whereas the measurement frequency resolution is ultimately determined by

the inverse of the TL aperture. The improved performance offered by the nonlinear-optics TL with respect to the EO implementation is, however, achieved at the expense of significantly higher power requirements and more complex setups. The TL scheme based on EO modulation of the microwave SUT onto a chirped optical waveform, Fig. 3(c), can offer a set of specifications (chirp, aperture) similar to the nonlinear-optics designs, with demonstrated frequency resolutions into the sub-GHz range [53], but without the stringent optical power requirements of the nonlinear approach.

## B. FTM Through Periodic Sampling

A different class of solutions for photonics-based RF Fourier processing is based on the use of optical sampling, in relation to the Talbot self-imaging effect [79,80]. When a periodic diffraction grating is illuminated by a plane wave, the intensity of the diffracted light in the vicinity of the grating maps the grating transmission function at specific propagation distances, namely, at integer multiples of the so-called Talbot length; similar “self-images,” but with a multiplied periodicity, are observed at propagation distances equal to a fractional multiple of the Talbot distance [81–83]. A temporal version of the Talbot effect arises in the propagation of a train of phase-locked optical pulses through a specific amount of GVD [84], an effect that has been exploited for multiplication of the repetition rate of pulsed lasers [85,86]. When the input optical pulse train is temporally modulated (in amplitude and/or phase) by a periodic RF SUT, the instantaneous power in the Talbot plane, i.e., the temporal profile of the resulting waveform, follows the discrete Fourier transform of the SUT [see Fig. 5(a)] [89,90]. This concept has been used for generation of high-repetition-rate periodic pulse trains with a reconfigurable, user-defined temporal envelope [91]. Perhaps most importantly, it has been recently shown that a similar scheme involving optical sampling of the microwave SUT followed by GVD can also be used for real-time spectral analysis of arbitrary RF signals, not restricted to the case of periodic waveforms only, in an entirely dynamic and continuous fashion. In particular, the output of this system maps along the temporal domain a representation of the full spectrogram (frequency spectrum versus time) of the input SUT as the signal is processed by the system [87]. Figure 5(b) shows experimental results of photonic-based time-mapped spectrogram analysis of a chirped microwave signal, with a frequency varying from 500 MHz to 2.43 GHz. The analysis was conducted with a resolution of  $\sim 340$  MHz.

The Talbot effect can be interpreted as the coherent addition of the wavefronts diffracted by the individual grating apertures. In the corresponding time-domain equivalent, multiple replicas of the light waveform modulated by the SUT, shifted in both time and in frequency, are coherently added to produce the resulting waveform. This process can be achieved without the use of GVD in a recirculating frequency-shifting loop (FSL), i.e., a fiber loop comprising an acousto-optic frequency shifter [92] [see Fig. 5(c)]. First the RF SUT is applied to a CW laser by an EO modulator and then coupled to the FSL. Provided that a certain relationship is satisfied between the time shift (i.e., the round-trip time) and the acousto-optic frequency shift, the output instantaneous power maps the power spectrum of the SUT. This new FTM technique—later extended to the fractional Fourier transform of RF signals in real time [93]—has shown a record frequency resolution in the

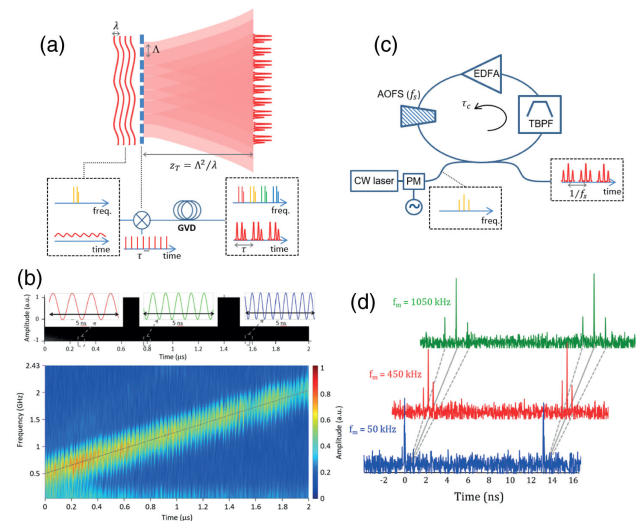


**Fig. 5.** Fourier analysis through periodic sampling. (a) A periodic waveform (wavelength  $\lambda$ ) is sampled by a transmission grating. For specific propagation distances (e.g., the Talbot length  $z_T$ ), the intensity maps repeatedly the input angular spectrum. In the time domain, the process is equivalent to sampling followed by GVD. (b) Demonstration of real-time spectrogram analysis by temporal sampling and GVD (bottom plot, showing the evolution of the time-mapped spectrum, vertical axis, along the time domain, horizontal axis) of an input linearly chirped microwave signal (top plot) [87]. (c) Fourier analysis based on FSL: the interference of replicas of the SUT, simultaneously shifted in both time and frequency, results in a time trace mapping the input signal frequency spectrum. (d) Example of high-resolution FTM in a FSL for input microwave tones of different frequency values,  $f_m$ . Adapted with permission from [88] © The Optical Society.

kHz range, and a minimum latency time set by the inverse of the achieved frequency resolution [see results in Fig. 5(d)] [88].

## C. On-Chip Integration of FTM Techniques

The main difficulty for integration of FTM techniques remains in the design and fabrication of compact (sub-cm) dispersive lines. Some solutions have been proposed, including coupled chirped vertical gratings [94–96], silicon waveguides [97], and nanophotonic waveguides or resonators [98,99]. Nonetheless, these technologies cannot provide the needed large amounts of GVD over broad operation bandwidths, in a short propagation length, suitable for chip-scale integration. To our knowledge, the first integrated optical D-FTM system, capable of computing the Fourier transform of pulses with up to 20 ps durations, was demonstrated in a silica glass [100]; however, SiP-compatible solutions remain to be demonstrated with the needed specifications for realization of dispersion-based FTM of microwave signals, i.e., capable of providing a frequency resolution at least within the sub-GHz range (corresponding to durations exceeding 1 ns).

On the other hand, integration of FSL-based approaches could be foreseeable. The passive building blocks of the FSL, such as the waveguides, couplers, and bandpass filters, are readily accessible through standard SiP foundries [26], while the lasers and amplifiers could be implemented through hybrid integration strategies [101]. Finally, integrated frequency shifters can be implemented through serrodyne phase modulation in silicon [102], or through EO single-sideband modulation in lithium niobate [103], or in

silicon [104]. This way, FSL architectures could provide a feasible path to integration of microwave FTM processors.

#### 4. PHOTONICS-BASED INSTANTANEOUS RF FREQUENCY MEASUREMENT SYSTEMS

A number of important applications do not require a full measurement of the entire SUT spectrum, but rather extracting some of its parameters only. In particular, many applications rely on the capability to measure the instantaneous frequency—the carrier or central frequency—of the incoming unknown RF signal over a large and continuous frequency span—from a few MHz up to the GHz range and beyond—in a rapid and accurate manner. Some examples include biomedical instrumentation [105], systems for monitoring radar environments [106], electronic countermeasures [107], etc. To this scope, so-called instantaneous frequency measurement (IFM) systems have been successfully employed since the 1950s.

Important figures of merit of photonic IFM systems include operation bandwidth, frequency resolution, variance and maximum error of estimation, sensitivity (i.e., the minimum detectable RF signal level), minimum required optical power, latency, capability of detecting multiple simultaneous unknown frequencies, and, last but not least, SWaP-C. A comprehensive review of the implementations of IFM systems and their evolution over the years into advanced digital IFM (DIFM) and all-digital systems was reported in Ref. [108]. However, even state-of-the-art DIFM are generally limited in their maximum frequency of identification. As mentioned above, direct digitization of microwave signals becomes challenging above  $\sim 20$  GHz [14].

To overcome this limitation, photonic IFM systems were first reported in the mid-2000s [109]. While the very first demonstrations offered similar overall performance compared to their all-electronic counterparts, the newly introduced concepts of operation, leveraging various photonic techniques, opened the way towards a series of developments that ultimately enabled remarkable performance improvements for IFM systems. In particular, the most reliable and highest-performing photonic IFM systems proposed to date are based on integrated optics platforms, following the general trend of current MWP technologies. Multiple approaches have been proposed for the implementation of integrated photonic IFM systems, which can be classified based on whether they rely on linear or nonlinear optics phenomena.

##### A. Linear Optics Approaches to Photonic IFM

###### 1. Frequency-to-Power Mapping Approach

Historically, the first photonic IFM systems proposed were based on optical filtering, in particular, on optical interferometers, reproducing the typical approach used in all-electronic IFM [108]. In this scheme, the RF SUT, whose unknown frequency is to be identified, modulates an OC, and it is then processed by one or more optical filters, prior to photodetection (see general scheme in Fig. 1). Frequency identification is achieved by exploiting the frequency dependency of the filter's transfer function to induce a corresponding RF-frequency-dependent attenuation of the modulation sideband. As a result, the photodetected RF power becomes a function of the sideband attenuation, resulting in a frequency-to-power-mapping process of the SUT, where the mapping law is given by the transfer function of the optical filter.

The correspondence between photodetected power and SUT frequency is unambiguous if the filter transfer function has a nonzero slope that does not change sign over the desired frequency range. Often, this frequency-to-power mapping is obtained as the ratio of different filter responses featuring opposite slopes. This is done in order to increase the system frequency estimation accuracy, and the relationship is generally known as the amplitude comparison function (ACF).

Different types of filters have been proposed and evaluated. Relatively simple examples include optical interferometers, where the modulated signal is split into two parts, which are sent through different optical delays and then recombined at the photodetector, creating an RF-frequency-dependent power response.

###### Implementations utilizing optical state of polarization.

Several demonstrations are based on interferometers operating in the polarization domain. In these systems, the different group velocities experienced by different polarizations of light in a birefringent medium or transmission line (the most common being a polarization-maintaining fiber) create an RF-frequency-dependent interference pattern, which, in turn, is used for frequency discrimination. Implementations using the differential group delay of a polarization-maintaining fiber were shown, e.g., up to 26 GHz [110], and covering the 1–18 GHz range with peak frequency error below 200 MHz [111]. Another implementation was demonstrated operating up to 40 GHz [112]. In Ref. [113], the RF frequency is derived from the evolution of the Stokes parameters at the output of a birefringent medium. [114] reports a system where measurement range and resolution can be adjusted by varying the angle between the principal axis of a polarization beam splitter and one principal axis of a polarization modulator. Other examples leverage fading effects in optical fibers to create differential delay [115]. In Ref. [116], the authors propose a concept using a polarization-maintaining fiber Bragg grating (PM-FBG) with different transmission profiles at different polarizations, where measurement range and resolution can be tuned by tuning the polarization angle. Recently, [117] reports an IFM system based on a dual-polarization dual-drive Mach–Zehnder modulator (Dpol-DMZM) where the upper and lower bounds of the frequency measurement range can be adjusted independently by adjusting the DC bias on both arms of the Dpol-DMZM.

**Tunable ring resonator implementation.** The first implementations of photonic IFM systems that made use of integrated filters were reported in Refs. [118,119]. The system reported in Ref. [118] was based on a compact programmable optical ring resonator (ORR), fabricated on a silicon nitride platform [see Figs. 6(a)–6(c)]. The SUT (modulated on an OC) was filtered by both the through and drop responses of the ORR filter, Fig. 6(b), to implement a frequency discriminator. The filtered signals were detected by separate photodiodes, and the ratio between the through and drop response determined the ACF [Figs. 6(d) and 6(e)]. In addition, tuning the quality factor of the ORR via micro-heaters allowed to modify the ACF range and slope, choosing the optimal tradeoff between measurement range and accuracy [Figs. 6(d)–6(g)]. The system is capable of estimating frequencies between 0.5 and 4 GHz with a standard deviation below 100 MHz. A version of this scheme employing a silicon micro-ring resonator was also reported [120]; this system could be tuned to feature either a broad bandwidth coverage, from 0.5 to 35 GHz, or high accuracy, as little as 63 MHz.

**Monolithic InP implementation.** The work reported in Ref. [119] demonstrated an IFM system using double-sideband

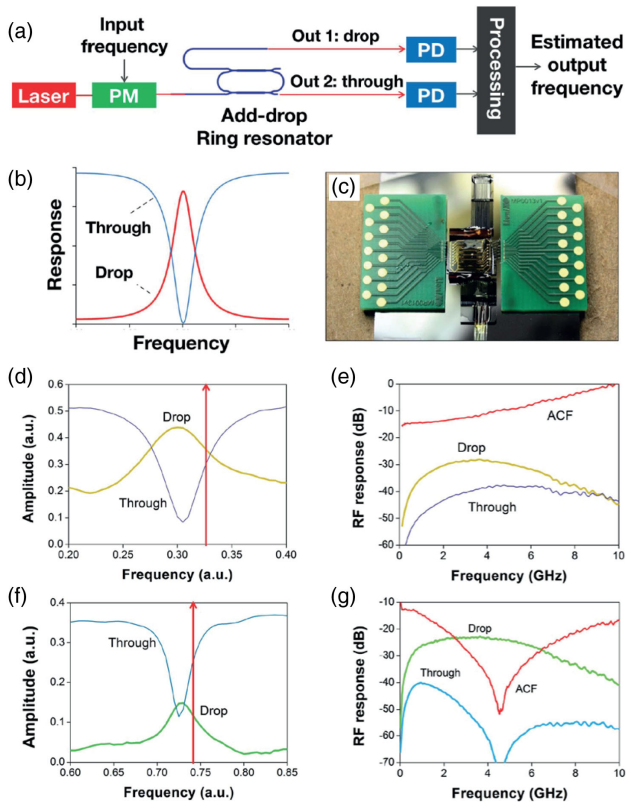


**Fig. 6.** Photonic IFM system using an on-chip frequency discriminator. (a) Experimental setup; (b) through and drop responses of the optical ring resonator filter; (c) photograph of the packaged chip. (d), (f) Position of the optical carrier (red arrow) with respect to the ORR responses; (e), (g) corresponding RF responses and ACF. Copyright 2013 IEEE. Reprinted with permission from [118].

suppressed-carrier modulation, where the optical filter—a ring-assisted Mach–Zehnder interferometer (RAMZI)—was integrated on an InP chip [Fig. 7(a)]. Aligning the carrier with the center of the bar response passband, Figs. 7(b)–7(c), the complementary bar and cross responses were used to determine the ACF [Figs. 7(d)–7(e)]. The system can identify frequencies between 5 and 15 GHz with a root mean square (RMS) error below 200 MHz. It should be noted that InP platforms may enable monolithic integration of active and passive photonic components (including lasers) to realize low SWaP-C photonic IFM systems [119].

**Waveguide Bragg grating implementation.** Photonic IFM implementations using on-chip discriminators based on resonant filters such as those reported above are generally limited in their maximum frequency range due to the finite FSR of the optical filters used. An alternative approach using non-frequency-periodic filters exploits the transmission and reflection responses of fiber Bragg gratings to create the ACF [121,122]. Recent works explored the potential of integrated waveguide Bragg grating filters (WBGs) to implement multiple MWP signal processing functions in a compact and low-power platform [23]. Among others, the possibility to replace ring- or fiber-based filters with WBGs to implement broadband, compact, and low-power IFM was shown. In particular, a novel, fully linear, low-optical-power (below 10 mW) IFM system was reported using an ultra-compact phase-shifted WBG on a silicon-on-insulator waveguide only 65  $\mu\text{m}$  long [Fig. 8(a)] [123]. The WBG is inserted into a MWP link based on single-sideband modulation [Fig. 8(b)]. The opposite responses used to define the

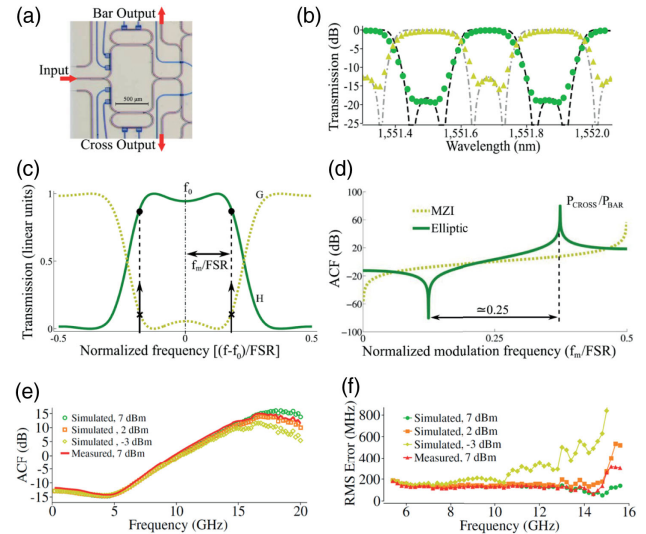


**Fig. 7.** Photonic IFM system based on a RAMZI filter. (a) Microscope photograph of the filter. (b) Simulated and measured bar (circles) and cross (triangles) responses. (c) Operation principle; (d) simulated and (e) measured ACF; (f) root-mean-square error. Adapted with permission from [119] © The Optical Society.

ACF are given by the transmission and reflection responses of the WBG, which can be accessed using separate dedicated waveguide output ports [Figs. 8(c)–8(d)]. Successful frequency identification up to 32 GHz with a standard deviation of approximately 755 MHz was demonstrated, limited by the amplified spontaneous emission (ASE) noise of the erbium-doped fiber amplifier (EDFA). This system has the potential for an unprecedented latency reduction, as low as tens of picoseconds. In addition, this photonic IFM was demonstrated for identification of frequency-varying signals dynamically, without fast measurement instrumentation [Fig. 8(e)]. Accurate frequency extraction was achieved up to 12 GHz, using a comparatively much-lower-speed electronic circuit, i.e., with a bandwidth below a few hundreds of MHz. This aspect, together with the low power and extreme compactness characteristics of the WBG, highlights the solid potential of this dynamic IFM system for a complete on-chip integration (possibly including active photonic elements).

## 2. Frequency-to-Time Mapping Approach

As discussed in Section 3, the frequency information of each tone of an RF SUT can be mapped to the time domain through FTM, using a scheme where different spectral components undergo different propagation delays. This concept was applied to IFM using a system comprising carrier-suppressed double-sideband modulation, time gating, and propagation through a dispersive medium [124]. The problem of frequency identification is then reduced to a problem of measuring relative time delays. In this work, a LC-FBG with a GVD of 1000 ps/nm was used as the dispersive medium, achieving correct identification of RF signals from 15 to 45 GHz with frequency errors originating from the group-delay ripple of the LC-FBG below 1.56 GHz.

## 3. Sagnac Loop Approach

A recent IFM implementation [125] makes use of phase modulation within a Sagnac loop. The system produces a DC output that is a function of the unknown RF frequency, thus requiring

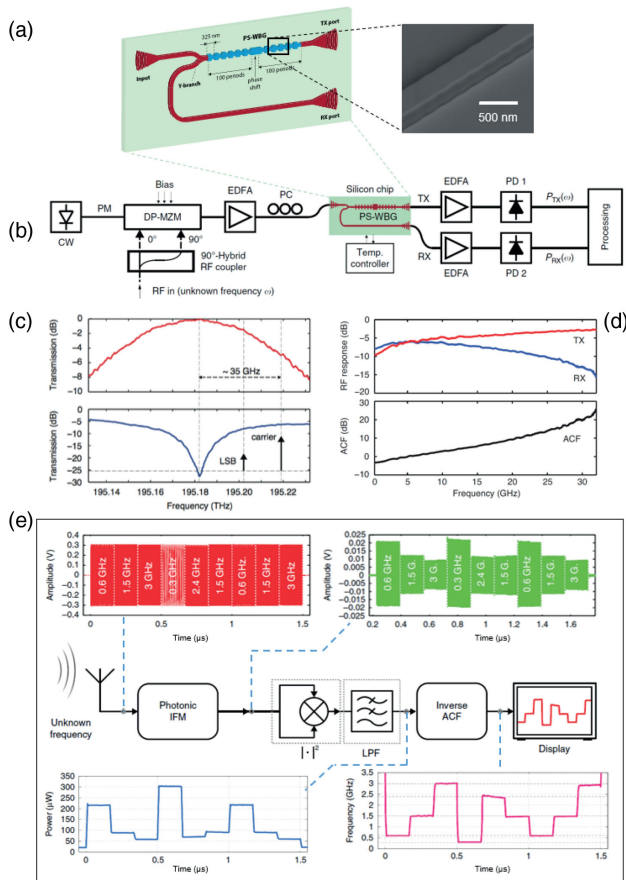


**Fig. 8.** Photonic IFM system based on WBG filter. (a) Schematic and scanning-electron microscope image of the WBG. (b) Experimental setup: CW, continuous-wave laser; PM, polarization-maintaining fiber; PC, polarization controller; DP-MZM, dual-parallel Mach-Zehnder modulator; EDFA, erbium-doped fibre amplifier; PS-WBG, phase-shifted waveguide Bragg grating; PD, photodetector; RX, reflection port; TX, transmission port. (c) Optical transmission from the TX (top) and RX (bottom) ports. (d) RF responses and ACF. (e) Dynamic frequency identification: (top-left) frequency-hopping RF SUT; (top-right) output amplitude encoding the SUT frequency; (bottom-left) instantaneous output signal power; (bottom-right) extracted time-varying frequency content of the SUT. Reproduced under the terms of the CC-BY Creative Commons Attribution 4.0 International License [123]. Copyright 2016, Macmillan Publishers Limited (now Springer Nature).

only a low-speed detector. It shows a range of 0.01–40 GHz, with less than 6% error for RF level as little as  $-30$  dBm and 10% at  $-51$  dBm. Not requiring long path lengths, this work may be suitable for on-chip integration as well.

## B. Nonlinear Optics Approaches to Photonic IFM

Nonlinear optics phenomena have been successfully leveraged to obtain IFM systems with particularly high selectivity and broad bandwidth.

### 1. Four-Wave-Mixing Approach

A first approach uses FWM in a highly nonlinear fiber (HNLF) [126]. A solution was proposed in which two equal-power OCs at different wavelengths are modulated by the same SUT and then delayed compared to each other via propagation through a

LC-FBG [112]. After proper optical amplification, they are sent through 1 km of HNLF, where they produce FWM idler tones. The idler power is a sinusoidal function of the RF frequency, and as a result, a simple low-speed photodetector can perform the desired IFM over the 1–40 GHz range. In a later work, the system capability was extended to independently measure both frequency and amplitude of the signal, up to 20 GHz [127]. In another implementation, the use of lock-in amplification allowed to increase the sensitivity and reach a 51 dB dynamic range, over a 0.04–40 GHz bandwidth with a 0.35% measurement error [128].

An important step forward was achieved in Ref. [129], which reports the first FWM-based IFM where the nonlinear medium—a 35 cm long spiral-shaped strip waveguide—was fully integrated on a SiP chip. A 0–40 GHz measurement bandwidth was achieved with an RMS error of 318.9 MHz (0.8% of the bandwidth). The system can also be reconfigured to work in a higher-accuracy mode by operating on 7.2 GHz sub-bands, further lowering the error to 40.2 MHz (0.52%).

### 2. Stimulated Brillouin Scattering Approach

The use of stimulated Brillouin scattering (SBS) was also proposed to implement IFM [130]. The concept performs single-sideband suppressed-carrier modulation of an optical CW by the RF frequency to be identified; the generated sideband is then used as a pump for the SBS process [126]. A probe signal is tuned to be at a fixed frequency shift from the pump, equal to the Brillouin shift plus a small detuning. Since the Brillouin shift depends on the pump frequency, the probe will experience a Brillouin gain that varies with the unknown frequency. The resulting probe power variation can be sensed with a low-speed photodetector. The demonstration used 2 km long SMF as the nonlinear medium and showed frequency identification up to 25 GHz with an error of 272 MHz ( $\sim 1\%$ ). A novel approach was presented [131] using an SBS-based notch filter with anomalously high rejection with a 1 km SMF to achieve frequency estimation of multiple frequencies with an error as low as 250 kHz [132]. Exploiting on-chip SBS [133], those methods open new possibilities for on-chip, wideband, and high-resolution photonic IFM.

## C. Other Approaches to Photonic IFM

A number of recent demonstrations have shown powerful approaches to fast and wideband RF spectrum analysis based on dual-comb interferometry [134–137]. These include recent work on a wideband staring receiver capable of detecting low-probability of intercept signals over a 40 GHz range. The RF SUT to be analyzed modulates an OC and is split and heterodyned with two separate electro-optically generated frequency combs with slightly mismatched repetition rates. The Vernier relationship between the combs assures that the down-converted signals obtained from the heterodyning occur at different frequencies and can be measured to retrieve the frequency of the SUT in real time and over transient signals as well [135]. Another related approach focused on on-chip realization, not requiring frequency shifting stages, pulse compression, or optical filtering, ripe for integration using, e.g., on-chip combs [138] and compact broadband modulators [139,140].

## 5. CONCLUSION

In this mini review, we have summarized the latest trends for photonic-assisted RF spectral measurement and monitoring, including approaches for coherent MWP spectrum-scanning receiver architectures, real-time spectral analysis based on FTM, and MWP-based IFM systems. These important measurement tools can benefit from the inherent frequency bandwidth advantage of photonic solutions to enable an overall performance that may be challenging to achieve otherwise. On-chip integration is a much-desired goal for these technologies as well. Promising progress in this direction has been recently reported, as reviewed herein. We have also discussed remaining important challenges to be addressed towards practical applications of these MWP solutions. These include the need to achieve significant improvements in some of the central specifications provided by these tools, such as in regard to their frequency resolution and/or reliability (measurement errors), or the realization of crucial components not yet available in compact integrated formats, such as the required highly dispersive lines for on-chip real-time RF spectral analysis. Research is under steady progress to address these challenges as well as to achieve full integration of the resulting measurement platforms, including the development of alternative design architectures, e.g., FSL-based FTM schemes, or digital feed-forward laser-noise-cancelling MWP receivers. Further studies are also needed to understand the potential of the MWP approach, and/or optimize the resulting MWP system designs, to provide the needed performance in terms of other important parameters, such as sensitivity and dynamic range under different noise conditions, according to the specific requirements of the target applications. The works discussed in this mini review clearly show the benefits that integrated MWP approaches could bring in the pursuit of future wideband microwave spectral measurement and monitoring schemes on-chip with unprecedented performance and capabilities.

**Funding.** Natural Sciences and Engineering Research Council of Canada; Fonds de Recherche du Québec – Nature et Technologies; Agence Nationale de la Recherche (ANR-14-CE32-0022); SNSF Ambizione (173996).

**Acknowledgment.** L.R.C., D.O., and J.A. acknowledge funding from Natural Sciences and Engineering Research Council of Canada (NSERC) and Fonds de Recherche du Québec – Nature et Technologies (FRQNT). H.G.C. acknowledges funding from Agence Nationale de la Recherche. M.B. acknowledges funding from SNSF Ambizione.

**Disclosures.** The authors declare no conflicts of interest.

## REFERENCES

1. D. M. Pozar, *Microwave Engineering* (Wiley, 2004).
2. H. Sobol, "Microwave communications—an historical perspective," *IEEE Trans. Microw. Theory Tech.* **32**, 1170–1181 (1984).
3. F. Neri, *Introduction to Electronic Defense Systems* (SciTech, 2006).
4. M. Golio and J. Golio, *RF and Microwave Applications and Systems* (CRC Press, 2007).
5. X. Zou, B. Lu, W. Pan, L. Yan, A. Stöhr, and J. Yao, "Photonics for microwave measurements," *Laser Photon. Rev.* **10**, 711–734 (2016).
6. H. Arslan, *Cognitive Radio, Software Defined Radio, and Adaptive Wireless Systems* (Springer, 2007).
7. C. Dantea, *Modern Communications Receiver Design and Technology* (Artech House, 2010).
8. A. De Martino, *Introduction to Modern EW Systems* (Artech House, 2012).
9. H. Sun, A. Nallanathan, C. X. Wang, and Y. F. Chen, "Wideband spectrum sensing for cognitive radio networks: a survey," *IEEE Wireless Commun.* **20**, 74–81 (2013).
10. R. M. Monroe, "Gigahertz bandwidth and nanosecond timescales: new frontiers in radio astronomy through peak performance signal processing," Ph.D. thesis (California Institute of Technology, 2018).
11. Tektronix, Inc., "Fundamentals of Real-Time Spectrum Analysis," <https://www.tek.com/primer/fundamentals-real-time-spectrum-analysis>.
12. Keysight Technologies, Inc., "Real-time spectrum analyzer (RTSA) X-series signal analyzers," <https://literature.cdn.keysight.com/litweb/pdf/5991-1748EN.pdf>.
13. J. Anzalchi, P. Inigo, and B. Roy, "Application of photonics in next generation telecommunication satellites payloads," *Proc. SPIE* **10563**, 1063–1071 (2017).
14. W. Anwajler, A. Zajdel, J. Kus, and J. Kampa, "High dynamic range octave-band microwave frequency measurement systems up to 18 GHz," in *12th International Conference on Microwaves and Radar (MIKON-98) (IEEE Cat. No. 98EX195)* (1998), pp. 653–657.
15. D. Marpaung, C. Roeloffzen, R. Heideman, A. Leinse, S. Sales, and J. Capmany, "Integrated microwave photonics," *Laser Photon. Rev.* **7**, 506–538 (2013).
16. L. R. Chen, "Silicon photonics for microwave photonics applications," *J. Lightwave Technol.* **35**, 824–835 (2017).
17. D. Marpaung, J. Yao, and J. Capmany, "Integrated microwave photonics," *Nat. Photonics* **13**, 80–90 (2019).
18. R. Maram, S. Kaushal, J. Azaña, and L. R. Chen, "Recent trends and advances of silicon-based integrated microwave photonics," *Photonics* **6**, 13 (2019).
19. J. Capmany and D. Novak, "Microwave photonics combines two worlds," *Nat. Photonics* **1**, 319–330 (2007).
20. T. Berceci and P. Herczfeld, "Microwave photonics—a historical perspective," *IEEE Trans. Microw. Theory Tech.* **58**, 2992–3000 (2010).
21. R. W. Ridgway, C. L. Dohrman, and J. A. Conway, "Microwave photonics programs at DARPA," *J. Lightwave Technol.* **32**, 3428–3439 (2014).
22. D. Pérez, I. Gasulla, and J. Capmany, "Toward programmable microwave photonics processors," *J. Lightwave Technol.* **36**, 519–532 (2018).
23. M. Burla, L. Romero Cortés, M. Li, X. Wang, L. Chrostowski, and J. Azaña, "Integrated waveguide Bragg gratings for microwave photonics signal processing," *Opt. Express* **21**, 25120–25147 (2013).
24. M. Smit, K. Williams, and J. van der Tol, "Past, present, and future of InP-based photonic integration," *APL Photon.* **4**, 050901 (2019).
25. D. J. Blumenthal, R. Heideman, D. Geuzebroek, A. Leinse, and C. Roeloffzen, "Silicon nitride in silicon photonics," *Proc. IEEE* **106**, 2209–2231 (2018).
26. B. Jalali and S. Fathpour, "Silicon photonics," *J. Lightwave Technol.* **24**, 4600–4615 (2006).
27. X. Wu and K. Sengupta, "On-chip THz spectroscope exploiting electromagnetic scattering with multi-port antenna," *IEEE J. Solid-State Circuits* **51**, 3049–3062 (2016).
28. A. Agarwal, T. Banwell, and T. K. Woodward, "Optically filtered microwave photonic links for RF signal processing applications," *J. Lightwave Technol.* **29**, 2394–2401 (2011).
29. K.-Y. Tu, M. S. Rasras, D. M. Gill, S. S. Patel, Y.-K. Chen, A. E. White, A. Pomerene, D. Carothers, J. Beattie, M. Beals, J. Michel, and L. C. Kimerling, "Silicon RF-photonic filter and down-converter," *J. Lightwave Technol.* **28**, 3019–3028 (2010).
30. T. Shao, F. Parésys, G. Maury, Y. L. Guennec, and B. Cabon, "Investigation on the phase noise and EVM of digitally modulated millimeter wave signal in WDM optical heterodyning system," *J. Lightwave Technol.* **30**, 876–885 (2012).
31. D. Onori, F. Scotti, F. Laghezza, M. Bartocci, A. Zaccaron, A. Tafuto, A. Albertoni, A. Bogoni, and P. Ghelfi, "A photonically-enabled compact 0.5–26.5 GHz RF scanning receiver," *J. Lightwave Technol.* **36**, 1831–1839 (2018).
32. D. Onori, B. Crockett, A. Samani, D. V. Plant, and J. Azaña, "0–40 GHz-tunable RF receivers on chip exploiting a noise-cancelling architecture and a silicon photonic modulator," in *Optical Fiber Communication Conference (OFC)* (2018).

33. D. Onori, F. Laghezza, P. Ghelfi, A. Bogoni, A. Albertoni, and A. Tafuto, "A photonics-based ultra wideband scanning RF receiver with high sensitivity and dynamic range," in *IEEE International Topical Meeting on Microwave Photonics* (2015).
34. J. R. Adleman, C. L. Lin, S. B. Jester, B. M. Pascoguin, D. C. Evans, and E. W. Jacobs, "Photonic RF-IF wideband down conversion using optical injection locking," *Proc. SPIE* **9467**, 946721 (2015).
35. D. Onori and J. Azaña, "A microwave photonic tunable receiver with digital feed-forward phase noise cancellation for electronic support measures and antenna remoting," in *IEEE International Topical Meeting on Microwave Photonics* (2018).
36. I. Fatadin, S. J. Savory, and D. Ives, "Compensation of quadrature imbalance in an optical QPSK coherent receiver," *IEEE Photon. Technol. Lett.* **20**, 1733–1735 (2008).
37. T. R. Zaman, X. Guo, and R. J. Ram, "Semiconductor waveguide isolators," *J. Lightwave Technol.* **26**, 291–301 (2008).
38. D. Onori, A. Samani, D. V. Plant, and J. Azaña, "An RF scanning receiver on a silicon photonic chip," in *IEEE International Topical Meeting on Microwave Photonics* (2019).
39. C. Dorrer and D. N. Maywar, "RF spectrum analysis of optical signals using nonlinear optics," *J. Lightwave Technol.* **22**, 266–274 (2004).
40. M. Pelusi, F. Luan, T. D. Vo, M. R. E. Lamont, S. J. Madden, D. A. Bulla, D.-Y. Choi, B. Luther-Davies, and B. J. Eggleton, "Photonic-chip-based radio-frequency spectrum analyser with terahertz bandwidth," *Nat. Photonics* **3**, 139–143 (2009).
41. P. Berger, Y. Attal, M. Schwarz, S. Molin, A. Louchet-Chauvet, T. Chanelière, J.-L. Le Gouët, D. Dolfi, and L. Morvan, "RF spectrum analyzer for pulsed signals: ultra-wide instantaneous bandwidth, high sensitivity, and high time-resolution," *J. Lightwave Technol.* **34**, 4658–4663 (2016).
42. D. J. Esman, V. Ataie, B. P.-P. Kuo, E. Temprana, N. Alic, and S. Radic, "Comb-assisted cyclostationary analysis of wideband RF signals," *J. Lightwave Technol.* **35**, 3712–3719 (2017).
43. B. H. Kolner, "Space-time duality and the theory of temporal imaging," *IEEE J. Quantum Electron.* **30**, 1951–1963 (1994).
44. J. van Howe and C. Xu, "Ultrafast optical signal processing based upon space-time dualities," *J. Lightwave Technol.* **24**, 2649–2662 (2006).
45. V. Torres-Company, J. Lancis, and P. Andrés, "Space-time analogies in optics," *Prog. Opt.* **56**, 1–80 (2011).
46. R. Salem, M. A. Foster, and A. L. Gaeta, "Application of space-time duality to ultrahigh-speed optical signal processing," *Adv. Opt. Photon.* **5**, 274–317 (2013).
47. B. E. A. Saleh and M. C. Teich, *Fundamentals of Photonics* (Wiley, 2019).
48. M. A. Muriel, J. Azaña, and A. Carballar, "Real-time Fourier transformer based on fiber gratings," *Opt. Lett.* **24**, 1–3 (1999).
49. J. Azaña and M. A. Muriel, "Real-time optical spectrum analysis based on the time-space duality in chirped fiber gratings," *IEEE J. Quantum Electron.* **36**, 517–526 (2000).
50. A. Weiner, *Ultrafast Optics* (Wiley, 2011).
51. G. P. Agrawal, *Nonlinear Optics* (Academic, 2012).
52. K. Goda, A. Mahjoubfar, C. Wang, A. Fard, J. Adam, D. R. Gossett, A. Ayazi, E. Sollier, O. Malik, E. Chen, Y. Liu, R. Brown, N. Sarkhosh, D. D. Carlo, and B. Jalali, "Hybrid dispersion laser scanner," *Sci. Rep.* **2**, 445 (2012).
53. R. E. Saperstein, D. Panasencko, and Y. Fainman, "Demonstration of a microwave spectrum analyzer based on time-domain optical processing in fiber," *Opt. Lett.* **29**, 501–503 (2004).
54. V. Torres-Company, D. E. Leaird, and A. M. Weiner, "Dispersion requirements in coherent frequency-to-time mapping," *Opt. Express* **19**, 24718–24729 (2011).
55. S. Dobner and C. Fallnich, "Dispersive Fourier transformation femtosecond stimulated Raman scattering," *Appl. Phys. B* **122**, 1–6 (2016).
56. C. Wang and J. Yao, "Ultrahigh-resolution photonic-assisted microwave frequency identification based on temporal channelization," *IEEE Trans. Microw. Theory Tech.* **61**, 4275–4282 (2013).
57. K. Goda and B. Jalali, "Dispersive Fourier transformation for fast continuous single-shot measurements," *Nat. Photonics* **7**, 102–112 (2013).
58. K. Krupa, K. Nithyanandan, U. Andral, P. Tchofo-Dinda, and P. Grelu, "Real-time observation of internal motion within ultrafast dissipative optical soliton molecules," *Phys. Rev. Lett.* **118**, 243901 (2017).
59. C. Wang, "Dispersive Fourier transformation for versatile microwave photonics applications," *Photonics* **1**, 586–612 (2014).
60. T. Jansson, "Real-time Fourier transformation in dispersive optical fibers," *Opt. Lett.* **8**, 232–234 (1983).
61. Corning, "SMF-28 Ultra optical fiber," 2014, <https://www.corning.com>.
62. R. Kashyap, *Fiber Bragg Gratings* (Academic, 2009).
63. K. O. Hill and G. Meltz, "Fiber Bragg grating technology fundamentals and overview," *J. Lightwave Technol.* **15**, 1263–1276 (1997).
64. E. D. Diebold, N. K. Hon, Z. Tan, J. Chou, T. Sienicki, C. Wang, and B. Jalali, "Giant tunable optical dispersion using chromo-modal excitation of a multimode waveguide," *Opt. Express* **19**, 23809–23817 (2011).
65. D. R. Solli, J. Chou, and B. Jalali, "Amplified wavelength-time transformation for real-time spectroscopy," *Nat. Photonics* **2**, 48–51 (2008).
66. J. D. Schwartz, J. Azaña, and D. V. Plant, "Experimental demonstration of real-time spectrum analysis using dispersive microstrip," *IEEE Microw. Wireless Compon. Lett.* **16**, 215–217 (2006).
67. C. Lei, B. Guo, Z. Cheng, and K. Goda, "Optical time-stretch imaging: principles and applications," *Appl. Phys. Lett.* **3**, 011102 (2016).
68. A. Mahjoubfar, D. V. Churkin, S. Barland, N. Broderick, S. K. Turitsyn, and B. Jalali, "Time stretch and its applications," *Nat. Photonics* **11**, 341–351 (2017).
69. A. Dezfooliyani and A. M. Weiner, "Photonic synthesis of high fidelity microwave arbitrary waveforms using near field frequency to time mapping," *Opt. Express* **21**, 22974–22987 (2013).
70. B. H. Kolner and M. Nazarathy, "Temporal imaging with a time lens," *Opt. Lett.* **14**, 630–632 (1989).
71. J. Azaña, N. K. Berger, B. Levit, and B. Fischer, "Simplified temporal imaging systems for optical waveforms," *IEEE Photon. Technol. Lett.* **17**, 94–96 (2005).
72. Z. Wu, L. Lei, J. Dong, J. Hou, and X. Zhang, "Reconfigurable temporal Fourier transformation and temporal imaging," *J. Lightwave Technol.* **32**, 4565–4570 (2014).
73. M. A. Foster, R. Salem, D. F. Geraghty, A. C. Turner-Foster, M. Lipson, and A. L. Gaeta, "Silicon-chip-based ultrafast optical oscilloscope," *Nature* **456**, 81–84 (2008).
74. A. W. Lohmann and D. Mendlovic, "Fractional Fourier transform: photonic implementation," *Appl. Opt.* **33**, 7661–7664 (1994).
75. C. Zhang, J. Xu, P. C. Chui, and K. K. Y. Wong, "Parametric spectro-temporal analyzer (PASTA) for real-time optical spectrum observation," *Sci. Rep.* **3**, 2064 (2013).
76. B. H. Kolner, "Chap. 19—Electro-optic time lenses for shaping and imaging optical waveforms, in *Broadband Optical Modulators: Science, Technology, and Applications* (CRC Press, 2011), pp. 427–453.
77. R. Salem, M. A. Foster, A. C. Turner, D. F. Geraghty, M. Lipson, and A. L. Gaeta, "Optical time lens based on four-wave mixing on a silicon chip," *Opt. Lett.* **33**, 1047–1049 (2008).
78. T. T. Ng, F. Parmigiani, M. Ibsen, Z. Zhang, P. Petropoulos, and D. J. Richardson, "Compensation of linear distortions by using XPM with parabolic pulses as a time lens," *IEEE Photon. Technol. Lett.* **20**, 1097–1099 (2008).
79. H. F. Talbot, "LXXVI. Facts relating to optical science. No. IV," *Philos. Mag.* **9**(56), 401–407 (1836).
80. H. F. Lord Rayleigh, "XXV. On copying diffraction-gratings, and on some phenomena connected therewith," *Philos. Mag.* **11**(67), 196–205 (1881).
81. K. Patorski, "I. The self-imaging phenomenon and its applications," *Prog. Opt.* **27**, 1–108 (1989).
82. M. V. Berry and S. Klein, "Integer, fractional and fractal Talbot effects," *J. Mod. Opt.* **43**, 2139–2164 (1996).
83. L. Romero Cortés, H. Guillet de Chatellus, and J. Azaña, "On the generality of the Talbot condition for inducing self-imaging effects on periodic objects," *Opt. Lett.* **41**, 340–343 (2016).
84. T. Jansson and J. Jansson, "Temporal self-imaging effect in single-mode fibers," *J. Opt. Soc. Am.* **71**, 1373–1376 (1981).
85. J. Azaña and M. A. Muriel, "Temporal Talbot effect in fiber gratings and its applications," *Appl. Opt.* **38**, 6700–6704 (1999).
86. J. Azaña and M. A. Muriel, "Temporal self-imaging effects: theory and application for multiplying pulse repetition rates," *IEEE J. Sel. Top. Quantum Electron.* **7**, 728–744 (2001).

87. S. Reddy, R. Maram, and J. Azaña, "On-the-fly time mapped full spectrogram analysis of high-speed non-stationary microwave signals," in *European Conference on Optical Communication (ECOC)*, Rome, Italy, 2018, pp. 1–3.
88. H. Guillet de Chatellus, L. Romero Cortés, and J. Azaña, "Optical real-time Fourier transformation with kHz resolutions," *Optica* **3**, 1–8 (2016).
89. S. Tainta, M. J. Erro, M. J. Garde, and M. A. Muriel, "Temporal self-imaging effect for periodically modulated trains of pulses," *Opt. Express* **22**, 15251–15266 (2014).
90. C. Fernández-Pousa, "A dispersion-balanced discrete Fourier transform of repetitive pulse sequences using temporal Talbot effect," *Opt. Commun.* **402**, 97–103 (2017).
91. Q. Xie and C. Shu, "Reconfigurable envelope generation of optical pulse train based on discrete Fourier transform," *IEEE Photon. Technol. Lett.* **30**, 242–245 (2018).
92. H. Guillet de Chatellus, L. Romero Cortés, and J. Azaña, "Arbitrary energy-preserving control of the line spacing of an optical frequency comb over six orders of magnitude through self-imaging," *Opt. Express* **26**, 21069–21085 (2018).
93. C. Schnébelin and H. Guillet de Chatellus, "Agile photonic fractional Fourier transformation of optical and RF signals," *Optica* **4**, 907–910 (2017).
94. D. T. H. Tan, K. Ikeda, R. E. Saperstein, B. Slutsky, and Y. Fainman, "Chip-scale dispersion engineering using chirped vertical gratings," *Opt. Lett.* **33**, 3013–3015 (2008).
95. D. T. H. Tan, K. Ikeda, and Y. Fainman, "Coupled chirped vertical gratings for on-chip group velocity dispersion engineering," *Appl. Phys. Lett.* **95**, 141109 (2009).
96. D. T. H. Tan, P. C. Sun, and Y. Fainman, "Monolithic nonlinear pulse compressor on a silicon chip," *Nat. Commun.* **1**, 116 (2010).
97. C. Turner, C. Manolatu, B. S. Schmidt, M. Lipson, M. A. Foster, J. E. Sharping, and A. L. Gaeta, "Tailored anomalous group-velocity dispersion in silicon channel waveguides," *Opt. Express* **14**, 4357–4362 (2006).
98. H. Liang, Y. He, R. Luo, and Q. Lin, "Ultra-broadband dispersion engineering of nanophotonic waveguides," *Opt. Express* **24**, 29444–29451 (2016).
99. K. Y. Yang, K. Beha, D. C. Cole, X. Yi, P. Del'Haye, H. Lee, J. Li, D. Y. Oh, S. A. Diddams, S. B. Papp, and K. J. Vahala, "Broadband dispersion-engineered microresonator on a chip," *Nat. Photonics* **10**, 316–320 (2016).
100. K. Dolgaleva, A. Malacarne, P. Tannouri, L. A. Fernandes, J. R. Grenier, J. Stewart Aitchison, J. Azaña, R. Morandotti, P. R. Herman, and P. V. S. Marques, "Integrated optical temporal Fourier transformer based on a chirped Bragg grating waveguide," *Opt. Lett.* **36**, 4416–4418 (2011).
101. G.-H. Duan, C. Jany, A. Le Liepvre, A. Accard, M. Lamponi, D. Make, P. Kaspar, G. Levaufre, N. Girard, J.-M. F. F. Lelarge, A. Descos, S. M. B. Ben Bakir, D. Bordel, S. Menezes, G. de Valicourt, S. Keyvaninia, G. Roelkens, D. Van Thourhout, D. J. Thomson, F. Y. Gardes, and G. T. Reed, "Hybrid III-V on silicon lasers for photonic integrated circuits on silicon," *IEEE J. Sel. Top. Quantum Electron.* **20**, 158–170 (2014).
102. Y. Li, S. Verstyuyt, G. Yurtsever, S. Keyvaninia, G. Roelkens, D. Van Thourhout, and R. Baets, "Heterodyne laser Doppler vibrometers integrated on silicon-on-insulator based on serrodyne thermo-optic frequency shifters," *Appl. Opt.* **52**, 2145–2152 (2013).
103. S. Shimotsu, S. Oikawa, T. Saitou, N. Mitsugi, K. Kubodera, T. Kawanishi, and M. Izutsu, "Single side-band modulation performance of a LiNbO<sub>3</sub> integrated modulator consisting of four-phase modulator waveguides," *IEEE Photon. Technol. Lett.* **13**, 364–366 (2001).
104. M. Laueremann, C. Weimann, A. Knopf, W. Heni, R. Palmer, S. Koeber, D. L. Elder, W. Bogaerts, J. Leuthold, L. R. Dalton, C. Rembe, W. Freude, and C. Koos, "Integrated optical frequency shifter in silicon-organic hybrid (SOH) technology," *Opt. Express* **24**, 11694–11707 (2016).
105. Y. Takeuchi, *Instantaneous Frequency Measurement System* (1976).
106. J. B. Tsui, *Microwave Receivers with Electronic Warfare Applications* (Wiley, 1986).
107. D. L. Adamy, *Introduction to Electronic Warfare Modeling and Simulation* (Institution of Engineering and Technology, 2006).
108. P. W. East, "Fifty years of instantaneous frequency measurement," *IET Radar Sonar Navig.* **6**, 112–122 (2012).
109. L. V. T. Nguyen and D. B. Hunter, "A photonic technique for microwave frequency measurement," *IEEE Photon. Technol. Lett.* **18**, 1188–1190 (2006).
110. X. Zou, H. Chi, and J. Yao, "Microwave frequency measurement based on optical power monitoring using a complementary optical filter pair," *IEEE Trans. Microw. Theory Tech.* **57**, 505–511 (2009).
111. M. V. Drummond, P. Monteiro, and R. N. Nogueira, "Photonic RF instantaneous frequency measurement system by means of a polarization-domain interferometer," *Opt. Express* **17**, 5433–5438 (2009).
112. L. A. Bui, M. D. Pelusi, T. D. Vo, N. Sarkhosh, H. Emami, B. J. Eggleton, and A. Mitchell, "Instantaneous frequency measurement system using optical mixing in highly nonlinear fiber," *Opt. Express* **17**, 22983–22991 (2009).
113. T. Mengual, B. Vidal, and J. Martí, "Photonic RF frequency measurement combining SSB-SC modulation and birefringence," *Opt. Commun.* **283**, 2676–2680 (2010).
114. H. Zhang and S. Pan, "Instantaneous frequency measurement with adjustable measurement range and resolution based on polarisation modulator," *Electron. Lett.* **49**, 248–250 (2013).
115. N. Shi, Y. Gu, J. Hu, Z. Kang, X. Han, and M. Zhao, "Photonic approach to broadband instantaneous microwave frequency measurement with improved accuracy," *Opt. Commun.* **328**, 87–90 (2014).
116. Y. Li, L. Pei, J. Li, Y. Wang, J. Yuan, and T. Ning, "Photonic instantaneous frequency measurement of wideband microwave signals," *PLoS One* **12**, e0182231 (2017).
117. C. Yang, W. Yu, and J. Liu, "Reconfigurable instantaneous frequency measurement system based on a polarization multiplexing modulator," *IEEE Photon. J.* **11**, 5500611 (2019).
118. D. Marpaung, "On-chip photonic-assisted instantaneous microwave frequency measurement system," *IEEE Photon. Technol. Lett.* **25**, 837–840 (2013).
119. J. S. Fandiño and P. Muñoz, "Photonics-based microwave frequency measurement using a double-sideband suppressed-carrier modulation and an InP integrated ring-assisted Mach-Zehnder interferometer," *Opt. Lett.* **38**, 4316–4319 (2013).
120. H. Shao, H. Yu, X. Jiang, J. Yang, and G. Roelkens, "Large bandwidth and high accuracy photonic-assisted instantaneous microwave frequency estimation system based on an integrated silicon microresonator," in *11th International Conference on Group IV Photonics (GFP)* (2014), pp. 47–48.
121. Z. Li, B. Yang, H. Chi, X. Zhang, S. Zheng, and X. J. Jin, "Photonic instantaneous measurement of microwave frequency using fiber Bragg grating," *Opt. Commun.* **283**, 396–399 (2010).
122. Z. Li, C. Wang, M. Li, H. Chi, X. Zhang, and J. Yao, "Instantaneous microwave frequency measurement using a special fiber Bragg grating," *IEEE Microw. Wireless Compon. Lett.* **21**, 52–54 (2011).
123. M. Burla, X. Wang, M. Li, L. Chrostowski, and J. Azaña, "Wideband dynamic microwave frequency identification system using a low-power ultracompact silicon photonic chip," *Nat. Commun.* **7**, 13004 (2016).
124. L. V. T. Nguyen, "Microwave photonic technique for frequency measurement of simultaneous signals," *IEEE Photon. Technol. Lett.* **21**, 642–644 (2009).
125. H. Emami, M. Hajjhashemi, S. E. Alavi, A. S. M. Supaat, and L. Bui, "Microwave photonics instantaneous frequency measurement receiver based on a Sagnac loop," *Opt. Lett.* **43**, 2233–2236 (2018).
126. R. W. Boyd, *Nonlinear Optics* (Academic, 2003).
127. L. A. Bui and A. Mitchell, "Amplitude independent instantaneous frequency measurement using all optical technique," *Opt. Express* **21**, 29601–29611 (2013).
128. H. Emami and M. Ashourian, "Improved dynamic range microwave photonic instantaneous frequency measurement based on four-wave mixing," *IEEE Trans. Microw. Theory Tech.* **62**, 2462–2470 (2014).
129. M. Pagani, B. Morrison, Y. Zhang, A. Casas-Bedoya, T. Aalto, M. Harjanne, M. Kapulainen, B. J. Eggleton, and D. Marpaung, "Low-error and broadband microwave frequency measurement in a silicon chip," *Optica* **2**, 751–756 (2015).
130. R. Pant, S. Shakthi, and A. Mishra, "Instantaneous frequency measurement using optical pump frequency based resonance shift," in *Asia Communications and Photonics Conference* (2016).
131. H. Jiang, D. Marpaung, M. Pagani, L. Yan, and B. J. Eggleton, "Multiple frequencies microwave measurement using a tunable Brillouin RF photonic filter," in *11th Conference on Lasers and Electro-Optics Pacific Rim (CLEO-PR)* (2015), pp. 1–2.
132. D. Marpaung, B. Morrison, M. Pagani, R. Pant, D.-Y. Choi, B. Luther-Davies, S. J. Madden, and B. J. Eggleton, "Low-power, chip-based

- stimulated Brillouin scattering microwave photonic filter with ultrahigh selectivity," *Optica* **2**, 76–83 (2015).
133. R. Pant, C. G. Poulton, D.-Y. Choi, H. McFarlane, S. Hile, E. Li, L. Thevenaz, B. Luther-Davies, S. J. Madden, and B. J. Eggleton, "On-chip stimulated Brillouin scattering," *Opt. Express* **19**, 8285–8290 (2011).
  134. A. Klee, C. Middleton, and R. DeSalvo, "Dual-comb spectrometer for fast wideband RF spectral analysis," in *IEEE Photonics Conference (IPC)* (2017), pp. 379–380.
  135. R. DeSalvo, A. Klee, C. Middleton, K. Bagnell, E. Grafer, and A. Cramer, "Advanced microwave photonics applications and routes to hybrid integration," in *Conference on Lasers and Electro-Optics (CLEO)*, OSA Technical Digest (online) (2018).
  136. M. S. Alshaykh, D. E. Leaird, J. D. McKinney, and A. M. Weiner, "Rapid wideband RF subsampling and disambiguation using dual combs," in *Conference on Lasers and Electro-Optics (CLEO)*, OSA Technical Digest (online) (2019).
  137. I. Coddington, N. Newbury, and W. Swann, "Dual-comb spectroscopy," *Optica* **3**, 414–426 (2016).
  138. P. Del'Haye, A. Schliesser, O. Arcizet, T. Wilken, R. Holzwarth, and T. J. Kippenberg, "Optical frequency comb generation from a monolithic microresonator," *Nature* **450**, 1214–1217 (2007).
  139. C. Wang, M. Zhang, X. Chen, M. Bertrand, A. Shams-Ansari, S. Chandrasekhar, P. Winzer, and M. Lončar, "Integrated lithium niobate electro-optic modulators operating at CMOS-compatible voltages," *Nature* **562**, 101–104 (2018).
  140. M. Burla, C. Hoessbacher, W. Heni, C. Haffner, Y. Fedoryshyn, D. Werner, T. Watanabe, H. Massler, D. Elder, L. R. Dalton, and J. Leuthold, "500 GHz plasmonic Mach-Zehnder modulator enabling sub-THz microwave photonics," *APL Photon.* **4**, 056106 (2019).